WPJET1-PR(17) 17878

C Guillemaut et al.

Experimental validation of an analytical kinetic model for Edge-Localized Modes in JET-ITER-Like Wall

Preprint of Paper to be submitted for publication in Nuclear Fusion

This work has been carried out within the framework of the EUROfusion Consortium and has received funding from the Euratom research and training programme 2014-2018 under grant agreement No 633053. The views and opinions expressed herein do not necessarily reflect those of the European Commission.

Experimental validation of an analytical kinetic model for Edge-Localized Modes in JET-ITER-Like Wall

*C. Guillemaut[1,2], C. Metzger[1,3], D. Moulton[4], K. Heinola[5], M. O'Mullane[6], I. Balboa[4], J. Boom[7], S. Silburn[4], E. Solano[8], G.F. Matthews[4] and JET contributors**

[1]EUROfusion Consortium, JET, Culham Science Centre, Abingdon, OX14 3DB, UK
[2]Instituto de Plasmas e Fusão Nuclear, Instituto Superior Técnico, Universidade Lisboa, PT
[3]Ambassade de France à Londres, 21 Cromwell Road, London SW7 2EN, UK
[4]CCFE, Culham Science Centre, Abingdon OX14 3DB, UK
[5]Department of Physics, University of Helsinki, P.O. Box 43, 00560 Helsinki, Finland
[6]Department of Physics, University of Strathclyde, Glasgow G4 0NG, UK
[7]Max-Planck-Institut fur Plasmaphysik, Boltzmannstr. 2, D-85748 Garching, Germany
[8]Laboratorio Nacional de Fusión, CIEMAT, 28040 Madrid, Spain
See the author list of "Litaudon et al, Nucl. Fusion **57 (2017) 102001"*
Contact Email: christophe.guillemaut@ukaea.uk or cguillemaut@ipfn.ist.utl.pt

Abstract

The design and operation of future fusion devices relying on H-mode plasmas requires reliable modelling of Edge-Localized Modes (ELMs) for precise prediction of divertor target conditions. The "Free-Streaming" kinetic model (FSM) used in this paper describes ELMs as a quasi-neutral plasma bunch expanding along the magnetic field lines into the Scrape-Off Layer without collisions. This allows for a simple analytical prediction of the time evolution of target plasma loads during ELMs. An extensive experimental validation of these predictions in more than 80 JET-ITER-Like Wall H-mode discharges with a wide range of conditions has been carried out here. Comparisons between diagnostic measurements of target ion flux density, power density, impact energy and electron temperature during ELMs with FSM predictions are presented in this paper and show excellent agreement.

1. Introduction

Predictions of target conditions such as power density, particle flux density and impact energy during Edge-Localized Modes (ELMs) in future fusion devices relying on H-mode plasmas is essential for the design of plasma facing components (PFC) and operational scenarios. Plasma-wall interaction issues like phase transition of the PFC material, erosion or impurity sputtering, are expected to be dominantly due to ELMs [1,2]. In this context, a reliable model allowing precise predictions of target conditions during ELMs to assess these phenomena would be very useful.

The "Free-Streaming" kinetic model (FSM) describes ELMs as a plasma bunch expanding along the magnetic field lines [3-5]. The model is based on the assumptions that ELMs are compact and conserve quasi-neutrality during their collisionless parallel transport from pedestal to targets. The FSM allows analytical calculations of the time evolution of target plasma loads during ELMs and could be a powerful predictive tool. To date, comparisons between FSM calculations of target power load or ion impact energy (E_i) with experimental measurements have been attempted on a very limited number of Type-I ELMy H-mode discharges and were successful in ASDEX-Upgrade and JET [2,4,6]. In order to confirm with confidence, the suspicion that key aspects of ELM physics are indeed captured by the FSM, a systematic and extensive validation effort has been carried out in JET-ITER-Like Wall (ILW) H-mode experiments and is presented in this paper. A data set comprising 82 JET-ILW Type-I or Type-III ELMy H-mode discharges with a very wide range of ELM frequency, input power (Fig. 1), plasma current, toroidal field and pedestal conditions have been used. These discharges were achieved with deuterium (D) or hydrogen as main species and a few of them involved nitrogen or neon seeding.

FSM predictions for the time evolution of target ion flux and power densities are tested for Type-I and Type-III ELMs in two representative JET-ILW H-mode cases in the next Section. The consequences of FSM physics on target electron and ion impact energy are discussed in Section 3 and 4, respectively. Finally, before concluding, the possible effects of energy reflection on target measurements during ELMs are discussed in the last Section 5.

2. Time evolution of target plasma loads during Type-I and Type-III ELMs

In the FSM, it is considered that the ELM filaments ejected upstream have a Maxwellian distribution of energy in both parallel and perpendicular directions. Since ELMy ions with the highest parallel energy free-stream faster to the targets than those with lower energy, it generates a characteristic time distribution of the ion and energy fluxes on the divertor targets. In a 1-D approach, ignoring potential cross-field transport effects, the strike-point surface ion flux ($\Gamma_\perp$ in A.m^{-2}) and power ($q_\perp$ in W.m^{-2}) densities predicted by the FSM [5] are respectively such that:

$$\Gamma_\perp = \Gamma_0 + \sin(\theta_\perp)\frac{e n_e^{ped}}{c_s}\frac{L_{//}L_{ELM}}{t^2}\exp\left(\frac{L_{//}^2}{2t^2c_s^2}\right) \quad (1)$$

and $$q_\perp = q_0 + \Gamma_\perp T_e^{ped}\left[\left(\frac{L_{//}}{c_s}\right)^2\frac{1}{t^2}+1\right], \quad (2)$$

with the background ion flux density Γ_0, the background power density q_0, the target field line angle $\theta_\perp \approx$ 2 – 3°, the pedestal electron density n_e^{ped} in m^{-3}, the pedestal electron temperature T_e^{ped} in eV, the sound speed $c_s = (2eT_e^{ped}/m_i)^{1/2}$, the ion mass m_i in kg, the time t in s, the target to target parallel connection length $L_{//}$ in m, the initial parallel extension of the ELM filaments L_{ELM} in m and e = 1.6x10^{-19} J.eV^{-1}. Here, the pedestal ion temperature is assumed to be equal to T_e^{ped} .

Fast divertor Langmuir probe (LP) and Infrared thermography (IR) measurements (Fig. 2) with a time resolution of 10 μs for $\Gamma_\perp$ and 200 μs for $q_\perp$, respectively, were available for the 82 discharges studied here. A coherent averaging method [7] using Beryllium II spectroscopy (Fig. 2) as an ELM marker has been used to obtain a typical average ELM time trace for each case. For convenience, detailed comparison of $\Gamma_\perp$ and $q_\perp$ experimental measurements with FSM calculations has been focused on two representative cases: discharge #84700 for typical large amplitude and slow Type-I ELMs with a frequency (f_{ELM}) of ≈ 50 Hz (Fig. 3a and c) and discharge #87588 for small amplitude and fast Type-III ELMs with f_{ELM} ≈ 1200 Hz (Fig. 3b and d). Fig. 3e and f are discussed latter on in this paper. Both parameters $L_{//}$ and L_{ELM} shown in Table 1 were adjusted in (1) and (2) to allow the best fit possible of the experimental $\Gamma_\perp$ and $q_\perp$ time traces. Mention should be made that the same $L_{//}$ and L_{ELM} values have been used in (1) and (2) and that the ELM compactness condition $L_{//}$ >> L_{ELM} for FSM validity is verified here. For the Type-I ELMs of #84700, L_{ELM} can be used to estimate the ELM energy (E_{ELM} in J) such that:

$$E_{ELM} \approx 3N_{fil}A_\perp\sqrt{2\pi}n_e^{ped}L_{ELM}eT_e^{ped} \qquad (3)$$

and verify its consistency with experiment. With the number of ELM filaments N_{fil} ≈ 10 [8,9] and the filament cross-section $A_\perp$ ≈ 3x10^{-3} m^2 [5,10], E_{ELM} ≈ 230 kJ which is close to the average variation of stored energy ΔW ≈ 200 kJ in this discharge. In #87588, we can estimate E_{ELM} ~ 1 kJ which is expected for small and fast Type-III ELMs. Unfortunately, the time resolution of ΔW measurements is not high enough to distinguish small periodic variations of this level.

The inter-ELM $L_{//}$ in JET-ILW is ~ 100 m which is close to the fitting parameter used for Type-III ELMs in #87588. However, $L_{//}$ must be more than ~ 8 times longer to allow a fit of the Type-I ELM time traces in Fig. 3a and c for #84700. During Type-I ELMs, perturbed $L_{//}$ of the order of ~ 5 - 10 times longer than the unperturbed inter-ELM value is already suggested by ELM simulations with the JOREK fluid code [11,12]. Similar fit attempt of a $q_\perp$ time trace from IR during Type-I ELMs in a JET-Carbon experiment also required significantly longer $L_{//}$ [4]. The JOREK code suggests that stochastisation of the magnetic field lines during Type-I ELM perturbations generate much longer paths for the ELMy ions than during inter-ELM. Since L_{ELM} is around ≈ 210 m in the large Type-I ELMs of #84700 compared to only ≈ 5 m in the small Type-III ELMs of #87588, it can be suspected that the increase of $L_{//}$ during an ELM depends on its size and the magnetic perturbation associated with it. The perturbation may simply be too small during Type-III ELMs to affect $L_{//}$ significantly.

Since the fits for $\Gamma_\perp$ and $q_\perp$ during Type-III ELMs in Fig. 3b and d involve Γ_0 = 700 A.m^{-2} and q_0 = 1 MW.m^{-2} respectively, it suggests that the coherently averaged signals for these quantities are built on top of a non-negligible background in these conditions. This is consistent with the peak values being only a small factor above the inter-ELM level. The background is negligible for the fit of the coherently averaged Type-I ELM signals.

3. Target electron energy during Type-I and Type-III ELMs

In Fig. 3a and b, the LP signals have been compared to D_α line emission from D recycling or desorption at the strike point calibrated with the number of ionization per Balmer photon (S/XB). These coherently averaged ionization rate densities have been obtained from D_α measurements accounting for the target electron density (n_e) and temperature (T_e) dependence of S/XB as given by the Atomic Data and Analysis Structure (ADAS) [13], see Fig. 4. If we assume that the increase of n_e during ELMs is proportional to $\Gamma_\perp$, n_e ranges from ≈ 2 to ≈ 5.3x10^{19} m^{-3} in #84700 and S/XB can be approximated by ≈ 3.33x10^{-19} n_e + 13.34 in this domain if $T_e \geq 30$ eV. In #87588, n_e ranges from ≈ 3 to ≈ 3.5x10^{18} m^{-3} where S/XB ≈ 13 if $T_e \geq 30$ eV. Since $T_e \geq 30$ eV during inter-ELM for both cases, it can be assumed that it will not be lower during ELMs.

If ELMy ions are essentially reflected as neutrals on the target and promptly re-ionized, the quantitative agreement between LP and calibrated D_α signals in Fig. 3a and b means that the recycling coefficient (R) during ELMs is near unity. If implantation dominates during ELMs, this match implies that the desorption rate of D neutrals from the near surface reservoir triggered by ELMs equals $\Gamma_\perp$ as if R = 1. This will be discussed in more details in Section 5 below.

In both eventualities, LP measurements are assumed to be valid during ELMs. However, it could be expected that ELMy electrons would have too much energy to be repelled by biased LP tips, preventing saturation of the ion current. In this case, the LP $\Gamma_\perp$ measurements should be significantly underestimated and lower than the calibrated D_α signals. The FSM provides an explanation for the validity of LP measurements during ELMs. To preserve quasi-neutrality in ELM filaments while they are transported to the target, electrons must transfer most of their parallel energy to the ions. This occurs very quickly much before the filaments reach the targets if the ELMs are sufficiently compact in the parallel direction, namely $L_{//} \gg L_{ELM}$ [5], which is verified here for both cases in Table 1. The electron perpendicular energy can also be transformed into parallel energy through electron-electron collisions and then transferred to the ions. This process is efficient if the electron collision time τ_e obtained as follows:

$$\tau_e = 3.45\times10^{11}\frac{T_{\parallel}^{3/2}}{n_e \ln\Lambda}A^2\left[-3+(A+3)\frac{\tan^{-1}(A^{1/2})}{A^{1/2}}\right]^{-1}, \quad (4)$$

with $A=\frac{T_e^{ped}}{T_{\parallel}}-1$, (5)

the Coulomb Logarithm $\ln\Lambda \approx 15.5$ here, and $T_{\|} = \dfrac{T_e^{ped}}{1+\left(0.556\dfrac{L_{\|}}{L_{ELM}}\right)^2}$, (6)

is such that τ_e << 0.556$L_{//}/c_s$ [5]. Since τ_e is not higher than 50 μs and 0.556$L_{//}/c_s$ ~ 1 ms in the cases studied here, most of the perpendicular energy of the electrons is transformed into parallel energy and then transferred to the ions.

The near complete transfer of parallel and perpendicular energy by the electrons to the ions during ELMs should allow them to be repelled by LP biasing when they reach the targets. Consequently, saturation of the ion current and T_e measurements should be possible during ELMs. These features have been verified here by reconstructing the current-voltage (I-V) characteristic in peak ELM conditions. Assuming that the I-V characteristic is close to:

$$I = I_{sat}(1-\mathrm{e}^{\frac{V-V_f}{T_{e,ELM}}}),\tag{7}$$

the saturation current I_{sat} in A, the floating potential V_f in V and the ELMy electron temperature $T_{e,ELM}$ in eV can be used as fitting parameters. As shown in Fig. 5, the fit gives $T_{e,ELM}$ ~ 30 eV during the Type-I ELMs of #84700 and $T_{e,ELM}$ ~ 40 eV during the Type-III ELMs of #87588 which correspond to the inter-ELM levels. Since T_e remains unchanged during ELM and inter-ELM, the assumptions made above about $n_e \propto \Gamma_\perp$ and $T_e \geq 30$ eV to estimate S/XB are confirmed. The presence of a single saturated I-V characteristic associated with low $T_{e,ELM}$ indicate that the electrons have indeed an energy low enough to allow current saturation of LPs during ELMs and valid $\Gamma_\perp$ measurements.

4. Target ion energy during Type-I and Type-III ELMs

Since the electron impact energy E_e can be neglected, E_i in eV can be calculated such as:

$$E_i + E_e \approx E_i \approx \frac{q_\perp}{\Gamma_\perp}.\tag{8}$$

The time evolution of E_i at the strike point is shown in Fig. 3e and f for cases #84700 and #87588. By dividing (2) by (1), the FSM predicts that at peak $q_\perp$, the maximum T_e^{ped} ($T_{e,\max}^{ped}$ in eV) and maximum E_i ($E_{i,max}$ in eV) are such as: $E_{i,max} \approx 5.23\,T_{e,\max}^{ped}$. Comparison between $E_{i,max}$ and coherently averaged $5.23\,T_{e,\max}^{ped}$ measurements in Fig. 3e and f indicates that both quantities seem close, as expected.

Coherent averaging of $\Gamma_\perp$ and $q_\perp$ measurements during Type-I and Type-III ELMs in 80 other cases has been carried out for calculation of $E_{i,max}$ at peak $q_\perp$ and systematic comparison with $T_{e,\max}^{ped}$. The fit method shown in Fig. 5 has also been applied to the rest of the cases studied here to obtain $T_{e,ELM}$ measurements and see if there is a correlation with $T_{e,\max}^{ped}$. A very wide range of pedestal conditions has been considered with $T_{e,\max}^{ped}$ going from ~ 170 eV to ~ 1500 eV. Fig. 6 shows a very clear linear trend following y = 5.23x for $E_{i,max} = f(T_{e,\max}^{ped})$ with some acceptable level of uncertainty. This good agreement confirms that the FSM equations (1) and (2) describe appropriately the experimental $\Gamma_\perp$ and $q_\perp$ time traces in the great variety of conditions of the 82 discharges considered here.

In the FSM picture, ELMy ions are essentially kinetic with a dominant parallel motion and the electrons do not have enough energy at the target to establish a sheath with a significant influence [5]. If ELM filaments were made of thermal ions and electrons with $T_{e,ELM} \approx T_{e,\max}^{ped}$, the electrons could establish a strong sheath with a heat transfer coefficient of $\gamma \approx 8$ [14] and we should have $E_{i,max} \approx \gamma T_{e,ELM}$. As shown in Fig. 6, the $T_{e,ELM}$ measurements are far too low to explain the very high $E_{i,max}$ observed in experiments. Therefore, sheath effects can be ignored during ELMs, as predicted by the FSM.

5. Discussion on energy reflections and deposition during ELMs

According to the TRIM database [15], the energy and particle reflection coefficients for D ions striking a smooth W surface with E_i in the range 1 - 10 keV are between 0.9 and 0.7. Consequently, most of impinging ELMy ions in the 82 cases studied here could be reflected as fast neutrals at the target and spread their energy over a wide area of the divertor without depositing significant amounts at the strike point. Therefore, $E_{i,max}$ calculated from IR and LP measurements in this region should not be higher than a few hundreds of eV. This is in contradiction with $E_{i,max}$ ranging from ~ 1 to nearly ~ 9 keV in Fig. 6, consistently with FSM predictions. Moreover, ELM energy depositions of the order of ~ ΔW on less than ~ 50 % of Tile 5 area (Fig. 2) are routinely found by IR measurements in JET-ILW [16,17]. This suggests that a large fraction of the ELM energy is indeed deposited on a limited area of the W PFC.

The reflection of high energy D particles (ions or neutrals) on W with shallow angle of incidence should be nearly specular [18]. After their first reflection, fast ELMy neutrals with a dominant toroidal motion and ~ 70 - 90 % of their initial ion energy can interact with the dense ELMy ion flow through charge exchange (CX), electron impact ionization and ion impact ionization. The mean free path deduced from ADAS [13] for a D fast neutral before the occurrence of a CX reaction is of the order of a few cm for ion densities $n_i \approx n_e$ ~ 10^{20} m^{-3} in the domain of energies 1 - 10 keV. On the other hand, electron impact ionization has a strong effect only at low energy and ion impact ionization is negligible. Therefore, most reflected fast neutrals can quickly become ions again through CX and come back to the target by following the magnetic field lines to leave more of their energy, see Fig. 7. ELMy particles could thus bounce back and forth between the target and the plasma and deposit their energy in the PFC by successive impacts and progressive implantations.

The remaining total energy of a fast ion population after a given number of reflections on W has been assessed with the SRIM code [19] using a binary collision approximation and the TRIM database [15]. For ions with an initial E_i = 5 keV and an angle of incidence of 5º with a smooth W surface, most of the total initial energy is deposited on the target after 5 – 6 reflections, see Fig. 8a. If surface roughness is considered, collisions with irregularities with a surface incidence angle up to 90º are possible. In this extreme case, most of the energy is deposited on the target after only 1 – 2 reflections, see Fig. 8b.

Observation of strong desorption associated with ELMs in JET-ILW [20-22] confirms that ELMy particles dominantly end up implanted after a few reflections. According to SRIM calculations [19], multi-keV D ions with shallow angles of incidence have an implantation depth of a few tens of nm in W. During ELMs, surface temperatures above 1000 ºC are measured by IR in JET-ILW and in these conditions, the mobility of implanted ELMy particles back to the surface should be fast with a diffusion time on the μs scale [23]. Therefore, the implantation of ELMy particles and the release of their energy should trigger the quasi-simultaneous fast diffusion and desorption of low energy D_2 molecules from the surface. The match between $\Gamma_\perp$ from LPs and the ionization rate density from calibrated D_α signals (Fig. 3a and b) implies that the implantation of a given amount of ELMy particles releases an equal amount of D neutrals. This recycling process is consistent with a saturated near surface reservoir expected with W PFCs [24].

Since the CX reaction conserves the charge, the initial charge carried by the ELMy ions leaving the pedestal should be the same as the charge carried by the fast ions impacting the target. Thus, $\Gamma_\perp$ measurements by LPs should not be affected by the multiple particle reflections and the slow ions produced after dissociation of D_2 molecules and electron ionization (Fig. 7) should be the main contributors to the background Γ_0 discussed in Section 2.

Since ELMy particle are very fast, the succession of impacts and CX reactions followed by implantation should not take more than a few μs. This is nearly instantaneous compared to the ELM duration which is usually of the order of a ms or more, see Fig. 3.

Quantitative description of the energy deposition mechanism on W during ELMs would require kinetic modelling of ELMy ions and neutrals accounting for the dominant atomic physics processes occurring in the plasma as well as the target properties. Such work is beyond the scope of this paper and should be the object of further studies.

6. Conclusions

The design and operation of plasma facing components in future fusion devices relying on ELMy H-mode plasmas requires reliable predictions of ELM power loads. The “Free-Streaming” model (FSM) allows analytical calculations of the time evolution of target plasma loads during ELMs [3-5] and could be used as a powerful predictive tool. Validation of the predictions of such model for 82 Type-I and Type-III ELMy H-mode discharges with a very wide range of conditions has been carried out with success in JET-ITER-Like Wall (ILW) and presented here.

It has been possible to fit the experimental time evolution of ELM power and particle flux densities at the strike point in typical Type-I and Type-III ELMy H-mode discharges in JET-ILW with the FSM. The parallel connection length and ELM length used as fitting parameters are consistent with the experimental ELM energy and with ELM modelling using the JOREK code [11,12].

FSM prediction of low target electron energy during ELMs due to near complete transfer of energy from electrons to ions to conserve quasi-neutrality has been verified in all Type-I and Type-III ELMy H-modes analysed here.

The ion impact energy at the strike point at peak power density ($E_{i,max}$) predicted by the FSM during ELMs matches the experimental estimates calculated from divertor infrared thermography (IR) and Langmuir probe measurements. As expected from the model, $E_{i,max}$ is proportional to the pedestal temperature before the ELM crash with a factor 5.23 and ranges from 1 keV to nearly 9 keV in the 82 cases studied here.

Tungsten is known to reflect very efficiently energetic ions at shallow angles of incidence [15] which suggests that energy deposition during ELMs should be spread on a very wide area of the divertor. In this picture, $E_{i,max}$ estimates at the strike-point should not exceed a few hundreds of eV. This is generally inconsistent ELM energy measurements from IR of the order of the variation of the stored energy on a limited area of JET-ILW divertor targets [16,17].

Charge exchange could force ELMy particles to bounce back and forth between the plasma and the target to allow efficient energy deposition by successive impacts and progressive implantations. Just a few reflections may be sufficient if surface roughness is considered. Full description of this mechanism would require kinetic modelling of ELMy ions and neutrals accounting for the atomic physics processes occurring in the plasma as well as the target properties. Such work is beyond the scope of this paper and should be the object of further studies.

Acknowledgments

This work has been carried out within the framework of the EUROfusion Consortium and has received funding from the Euratom research and training programme 2014-2018 under grant agreement No 633053. IST activities also received financial support from “Fundação para a Ciência e Tecnologia” through project UID/FIS/50010/2013. The views and opinions expressed herein do not necessarily reflect those of the IST or of the European Commission.

References

[1] J.P. Gunn *et al.*, Nuclear Materials and Energy (2016), http://dx.doi.org/10.1016/j.nme.2016.10.005
[2] C. Guillemaut *et al.*, Phys. Scr. T167 (2016) 014005
[3] W. Fundamenski *et al.*, Plasma Phys. Control. Fusion **48** (2006) 109–156
[4] T. Eich *et al.*, J. Nucl. Mater. **390–391** (2009) 760–763
[5] D. Moulton *et al.*, Plasma Phys. Control. Fusion **55** (2013) 085003
[6] C. Guillemaut et al., Plasma Phys. Control. Fusion **57** (2015) 085006
[7] R.A. Pitts *et al.*, Nucl. Fusion **43** (2003) 1145–1166
[8] R.A. Pitts *et al.*, Nucl. Fusion **46** (2006) 82
[9] M.W. Jakubowski *et al.*, J. Nucl. Mater. **390–391** (2009) 781
[10] A. Kirk *et al.*, J. Phys. Conf. Ser. **123** (2008) 012011
[11] S. Pamela *et al.*, Plasma Phys. Control. Fusion **58** (2016) 014026
[12] G.T.A. Huysmans *et al.*, Plasma Phys. Control. Fusion **51** (2009) 124012
[13] H.P. Summers. *Atomic data and analysis structure user manual*. University of Strathclyde, 2nd edition, 2004
[14] S. Marsen *et al.*, J. Nucl. Mat. **438** (2013) 393–396
[15] W. Eckstein *et al,* 2002 *Report IPP* 9/132
[16] A.R. Field *et al.,* Plasma Phys. Control. Fusion **59** (2017) 095003
[17] Private communication with L. Horvath
[18] W. Eckstein and D.B. Heifetz, J. Nucl. Mat. **145-147** (1987) 332
[19] J.F. Ziegler, Nucl. Instr. Meth. **B 268** (2010) 1818
[20] S. Wiesen *et al.*, Nucl. Fusion **57** (2017) 066024
[21] S. Brezinsek *et al.*, Phys. Scr. **T167** (2016) 014076
[22] Private communication with K. Heinola
[23] K. Heinola *et al*., Physical Review B **81** (2010) 073409
[24] S. Brezinsek *et al.*, J. Nucl. Mat. **463** (2015) 11–21

Figure captions :

Fig. 1 Range of power and ELM frequency in the Type-I or Type-III H-mode discharges studied here. These cases involved hydrogen or deuterium as main species.

Fig. 2 Magnetic equilibria for the Type-I (#84700) and Type-III (#87588) ELMy H-mode plasmas representative study and diagnostics involved.

Fig. 3 Examples of coherently averaged (a,b) $\Gamma_{\perp}$ from LPs (blue dots) and calibrated D_{α} (magenta squares), (c,d) $q_{\perp}$ (red dots), (e,f) E_i (green dots) and T_e^{ped} (black triangles) time traces for Type-I and Type-III ELMs in discharges #84700 and #87588 respectively. All target measurements are made at the strike-point. To facilitate the comparison with LPs, $\Gamma_{\perp}$ obtained from calibrated D_{α} is also in kA.m^{-2}. The dashed black curves in (a-c) are the FSM fits.

Fig. 4 n_e and T_e dependence of S/XB from ADAS [13].

Fig. 5 Example of *I*-*V* characteristic reconstructions (blues dots) and fits (red curves) during Type-I and Type-III ELMs in #84700 (left) and #87588 (right) respectively.

Fig. 6 Linear dependence between $E_{i,max}$ and $T_{e,\max}^{ped}$ during ELMs (red and blue bullets). No dependence can be found between $T_{e,ELM}$ and T_e^{ped} (red and blue squares). Red points correspond to Type-I ELMs experimental data and blue points to Type-III ELMs. The black line equation is $y = 5.23x$.

Fig. 7 Examples of atomic physics processes occurring at the target during ELMs.

Fig. 8 Remaining total energy of a fast ion population after a given number of reflections on W calculated with the SRIM code [19] for (a) 5º and (b) 90º surface incidence angles. The total reflected energy is normalized to the total initial energy.

Table caption:

Table 1 Experimental and fitting parameters for Type-I ELMs in #84700 and Type-III ELMs in #87588

	T_e^{ped} (eV)	n_e^{ped} (m^{-3})	$L_{//}$ (m)	L_{ELM} (m)
#84700	1000	$3x10^{19}$	864	210
#87588	550	$1.3x10^{19}$	112	5

Table 1

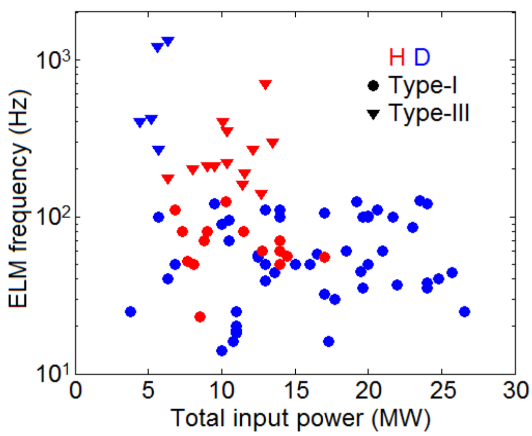

Fig. 1

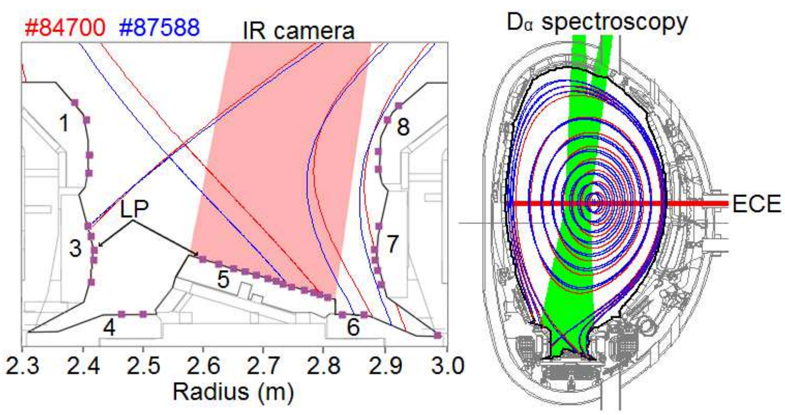

#84700 #87588
IR camera
1
8
LP
3
7
5
4
6
2.3 2.4 2.5 2.6 2.7 2.8 2.9 3.0
Radius (m)
Dα spectroscopy
ECE

Fig. 2

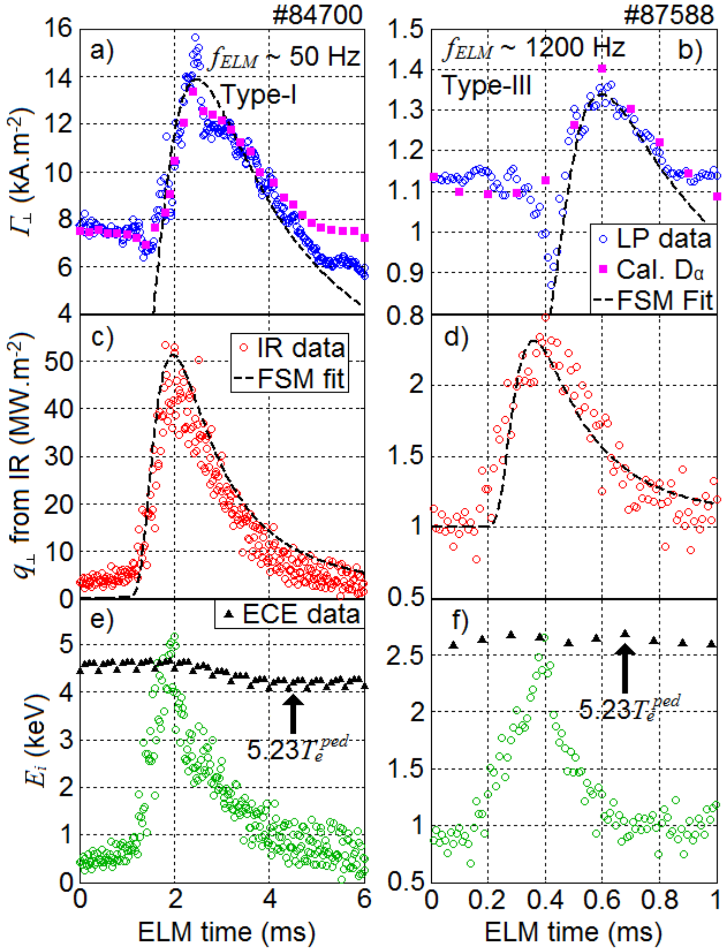

#84700
#87588
a)
f_{ELM} ~ 50 Hz
Type-I
f_{ELM} ~ 1200 Hz
b)
Type-III
LP data
Cal. Dα
FSM Fit
$\Gamma_\perp$ (kA.m^{-2})
c)
IR data
FSM fit
d)
$q_\perp$ from IR (MW.m^{-2})
e)
ECE data
f)
$5.23T_e^{ped}$
E_i (keV)
ELM time (ms)

Fig. 3

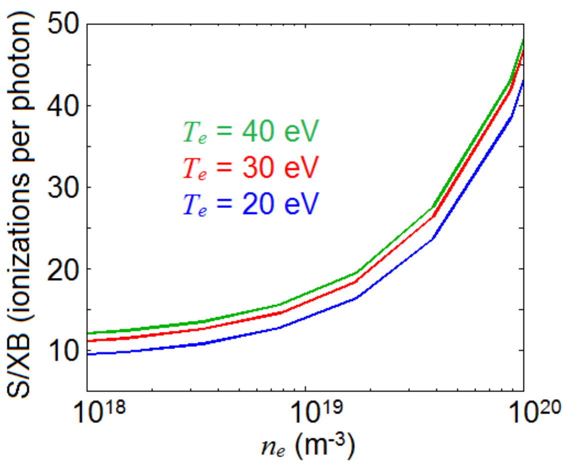

S/XB (ionizations per photon)
50
40
30
20
10
T_e = 40 eV
T_e = 30 eV
T_e = 20 eV
10^{18}
10^{19}
10^{20}
n_e (m^{-3})

Fig. 4

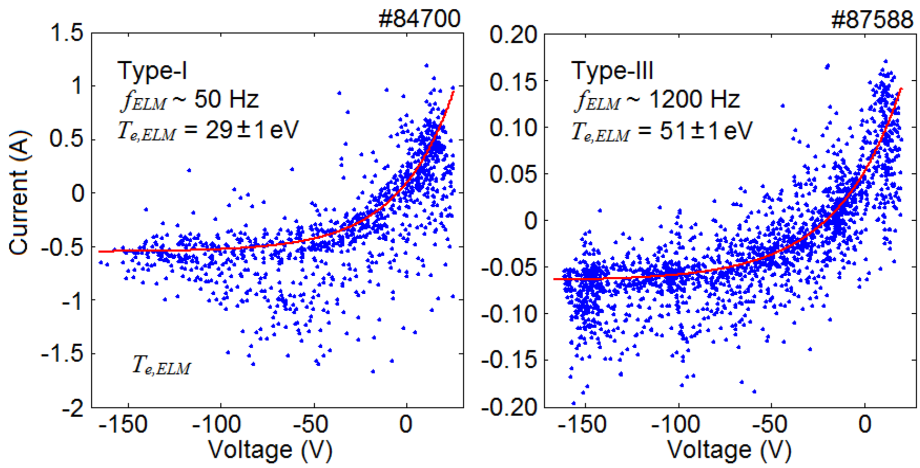
#84700
Type-I
f_{ELM} ~ 50 Hz
$T_{e,ELM}$ = 29±1 eV
$T_{e,ELM}$
Current (A)
Voltage (V)
#87588
Type-III
f_{ELM} ~ 1200 Hz
$T_{e,ELM}$ = 51±1 eV
Voltage (V)

Fig. 5

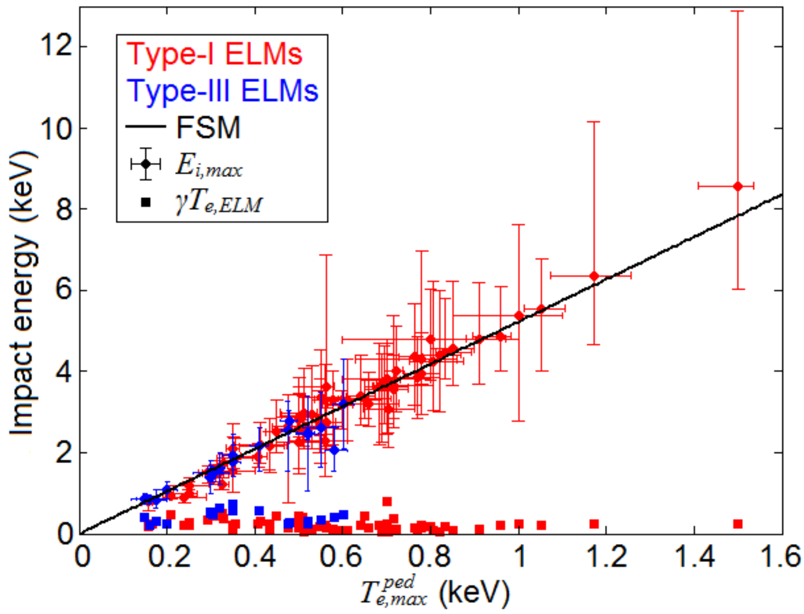

Type-I ELMs
Type-III ELMs
FSM
$E_{i,max}$
$\gamma T_{e,ELM}$
Impact energy (keV)
$T_{e,max}^{ped}$ (keV)
0
2
4
6
8
10
12
0.2
0.4
0.6
0.8
1
1.2
1.4
1.6

Fig. 6

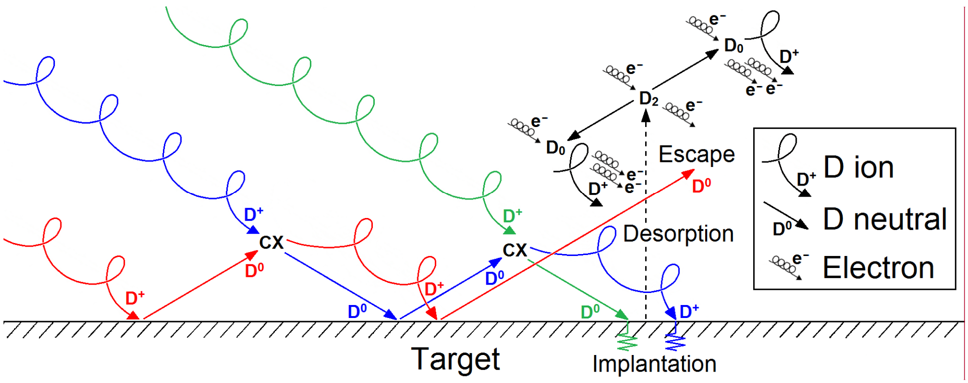

e⁻
D₀
D⁺
e⁻
D₂
e⁻
e⁻ e⁻
e⁻
D₀
e⁻
D⁺
e⁻
Escape
D⁰
D ion
D⁺
D neutral
D⁰
Electron
e⁻
Desorption
D⁺
CX
D⁰
D⁺
CX
D⁺
D⁰
D⁺
D⁰
D⁰
D⁰
D⁺
Target
Implantation

Fig. 7

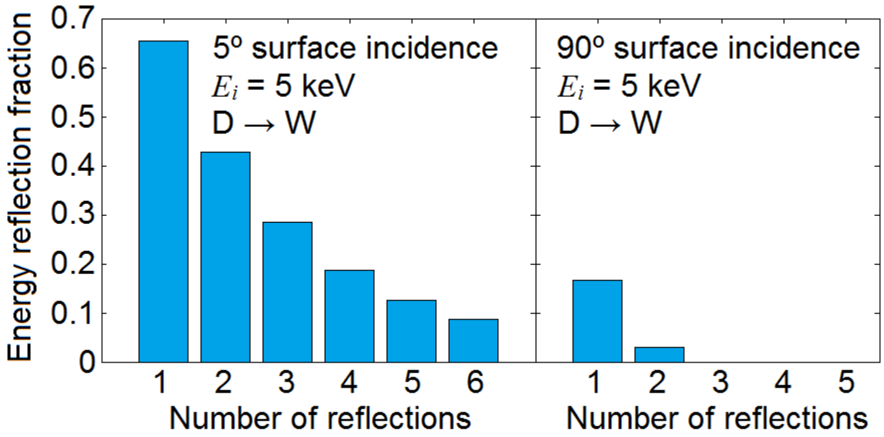
Energy reflection fraction
0.7
0.6
0.5
0.4
0.3
0.2
0.1
0
5° surface incidence
E_i = 5 keV
D → W
1 2 3 4 5 6
Number of reflections
90° surface incidence
E_i = 5 keV
D → W
1 2 3 4 5
Number of reflections

Fig. 8